




# Effects of Cr<sub>2</sub>O<sub>3</sub> nanoparticles on the chlorophyll fluorescence and chloroplast ultrastructure of soybean (*Glycine max*)

Jinxing Li<sup>1</sup> · Yuchao Song<sup>1</sup> · Keren Wu<sup>1</sup> · Qi Tao<sup>1</sup> · Yongchao Liang<sup>1</sup> · Tingqiang Li<sup>1</sup> 

Received: 10 October 2017 / Accepted: 25 April 2018 / Published online: 4 May 2018  
© Springer-Verlag GmbH Germany, part of Springer Nature 2018

## Abstract

Chromic oxide nanoparticles (Cr<sub>2</sub>O<sub>3</sub> NPs) are widely used in commercial factories and can cause serious environmental problems. However, the mechanism behind Cr<sub>2</sub>O<sub>3</sub> NP-induced phytotoxicity remains unknown. In this study, the effects of Cr<sub>2</sub>O<sub>3</sub> NPs on the growth, chlorophyll fluorescence, SEM-EDS analysis, and chloroplast ultrastructure of soybean (*Glycine max*) were investigated to evaluate its phytotoxicity. The growth of soybean treated with various Cr<sub>2</sub>O<sub>3</sub> NP suspensions (0.01, 0.05, 0.1, and 0.5 g L<sup>-1</sup>) was significantly inhibited. Specially, shoot and root biomass decreased by 9.9 and 46.3%, respectively. Besides, the maximum quantum yield of PSII (Fv/Fm) as well as the photochemical quenching (qP) decreased by 8–22 and 30–37%, respectively, indicating that the photosynthetic system was damaged when treated with Cr<sub>2</sub>O<sub>3</sub> NPs. Moreover, the inhibition was confirmed by the reduction of Rubisco and MDH enzyme activity (by 54.5–86.4 and 26.7–96.5%, respectively). Overall, results indicated that the damage was caused by the destruction of chloroplast thylakoid structure, which subsequently reduced the photosynthetic rate. Our research suggests that Cr<sub>2</sub>O<sub>3</sub> NPs can be transported and cause irreversible damage to soybean plants by inhibiting the activity of electron acceptors (NADP<sup>+</sup>) and destroying ultrastructure of chloroplasts, providing insights into plant toxicity issues.

**Keywords** Chlorophyll fluorescence · Photosynthesis · Photosynthetic enzymes · Cr<sub>2</sub>O<sub>3</sub> NPs

## Introduction

Metal oxide nanoparticles (NPs) have smaller size (particles with at least one dimension of less than 100 nm) and larger surface area, which lead to the unique physico-chemical patterns and high reactivity. NPs have recently been the focus of intense research because of its wide application in industrial, agricultural, and household use (Meshram et al. 2012; Zhu et al. 2004). Previous studies have proved that NPs can enter the environment via waste water from industrial sites or through domestic sewage (Hernandez-Viezcas et al. 2013;

Rico et al. 2011). Besides, NPs can be transported to soil via sewage sludge, then ultimately be absorbed by plants (Petersen et al. 2014), raising concerns to environmental safety and threat to plants (Hawthorne et al. 2014), living organisms, and even humans as a function of direct or indirect exposure (Rickerby and Morrison 2007; Ma et al. 2010).

The potential toxicity and bioaccumulation of NPs motivate the investigation of their fate and transportation in the uptake system. Plants are first produced in the ecosystem and may therefore easily act as intermediaries for the transfer of NPs to the organism (Hawthorne et al. 2014). It is reported that NPs can be species specific absorbed by various plants (Zhang et al. 2011; Wang et al. 2013; Ebbs et al. 2016a, b; Cui et al. 2014) and allocated to the roots, stems, and leaves (Harris and Bali 2008; Parsons et al. 2010; Navarro et al. 2008). Evidence showed that CeO<sub>2</sub> cannot be absorbed into maize through root resorption (Birbaum et al. 2010), but ZnO and CeO<sub>2</sub> can be accumulated into both shoot and root of soybean and corn. Besides, the accumulation of ZnO was higher than CeO<sub>2</sub> (Zhu et al. 2004; Priester et al. 2012; Zhao et al. 2012). Also, the cumulative amount of Ag NPs in soybean plant exposed to Ag NPs was significantly lower than

Responsible editor: Yi-ping Chen

**Electronic supplementary material** The online version of this article (<https://doi.org/10.1007/s11356-018-2132-x>) contains supplementary material, which is available to authorized users.

✉ Tingqiang Li  
litq@zju.edu.cn

<sup>1</sup> Ministry of Education Key Laboratory of Environmental Remediation and Ecological Health, College of Environmental and Resource Sciences, Zhejiang University, Hangzhou 310058, China

those in the plants exposed to CeO<sub>2</sub> NPs and ZnO NPs (De La Torre-Roche et al. 2013). Therefore, it is necessary to verify the uptake of different NPs in the plants.

Some studies argue that the varying degrees of toxicity responding to nanoparticles is related to the migration process inside the plants. CuO NPs can be transported to the shoots through xylem sap and translocated back to roots through phloem-based transport in maize (Wang et al. 2012), which is similar to Au NPs in woody poplar (Zhai et al. 2014), expressing a root-shoot-root distribution loop and providing evidence for the bioaccumulation and detoxification of NPs in plants. The migration process of NPs in plants may also be accompanied by ion release, change of redox state, combined with increased reactive oxygen species, thus resulting in irreversible damage to gene expression, causing root swelling and inhibition of root elongation (Wang et al. 2016; Ebbs et al. 2016a, b). In addition to morphology, changes in the valence of nanoparticles can be found in plants. The redox state of a small number of Cu were found to be changed from Cu(II) to Cu(I) in maize (Wang et al. 2012), and the redox state of a small part of Ce NPs were found to be reduced from Ce(IV) to Ce(III) in soybean (Hernandez-Viezcas et al. 2013); metal oxidation process is often accompanied with changes in plant organic metabolism, pH, and reactive oxygen species. CuO NPs were reported to raise reactive oxygen species (ROS) in rice (Shaw and Hossain 2013). In *Arabidopsis thaliana*, CuO NPs can cause the generation and accumulation of ROS in the chloroplasts, affecting the electron transfer, causing gene damage (Wang et al. 2016); Ag NPs were reported to induce the up-regulated expression of ROS-associated genes (Kohan-Baghkheirati and Geisler-Lee 2015).

However, most of the studies focused on the toxicity and crop yield reduction induced by NPs, only a few of them focused on the effects of nanoparticles on plant photosynthetic system. A life cycle experiment on cucumber pointed that NPs showed no effect on chlorophyll and gas exchange (Zhao et al. 2013), while CuO NPs were reported to cause damage to *Arabidopsis thaliana* chloroplasts, inhibiting the electron transfer during the photosynthetic process (Wang et al. 2016). Besides, the chlorophyll content was reported to be significantly reduced in wheat once exposed to ZnO NPs and CuO NPs (Dimkpa et al. 2012) but not significantly changed in soybean plants exposed to CeO<sub>2</sub> and ZnO (Zhao et al. 2013). Ag NPs only inhibited chlorophyll *b* content in rice (Mirzajani et al. 2013). In addition, TiO<sub>2</sub>, ZnO, and Au NPs were reported to enhance the chlorophyll content in some edible plants (Ma et al. 2015). To date, many studies only investigated the chlorophyll content and ROS damage, while only a small number of them have studied the changes in plant morphology and even less were focused on the ultrastructural changes. Photosynthesis-related organelles can be found by observing the subcellular structure of plants. Chlorophyll fluorescence imaging can visually show the damage of leaf

photosynthesis system, including electron transportation, opening degree of light system, as well as dark reaction rate. These two methods could provide an insight into the way that nanoparticles affect the photosynthesis of different plants.

Cr<sub>2</sub>O<sub>3</sub> is versatile as it is an excellent green dye material and stainless steel raw material (Farinati et al. 2011) and are used for industrial applications such as catalysts and pigments (Ondřej et al. 2014). In recent years, due to increasing technological requirements, the use of Cr<sub>2</sub>O<sub>3</sub> NP inputs was rising, especially in magnetic materials, refractories, and environmental catalysis (Park et al. 2016), but little attention has been paid to the environmental risks that Cr<sub>2</sub>O<sub>3</sub> NPs could pose to plants and even humans. The transportation form and the toxicity of Cr<sub>2</sub>O<sub>3</sub> NPs could pose to the growth, and photosynthesis of plants still remains uncertain. Soybean plants, as one of the largest farm species around the world, were chosen because of its popularity as food and also economical crops, which have direct connections with human life. To get a comprehensive understanding of the direct effects of nanoparticles on plants, SEM/TEM and CF Imager were conducted in the present study. Experiments were performed and differences in Cr<sub>2</sub>O<sub>3</sub> NP intensity were confirmed by various analyses. This study aimed to (1) confirm that Cr<sub>2</sub>O<sub>3</sub> NPs can be absorbed and translocated by soybean plants; (2) measure the activity of photosynthetic enzymes and observe the substructure damage of chloroplasts with the addition of Cr<sub>2</sub>O<sub>3</sub> NPs; (3) collect and analyze the photosynthetic data along with the chlorophyll fluorescence image to reveal the electron transport and the damage of dark reaction. The findings in this work will help to gain insight into the negative effects induced by Cr<sub>2</sub>O<sub>3</sub> NPs and provide evidence to assess the risk.

## Materials and methods

### Cr<sub>2</sub>O<sub>3</sub> nanoparticle suspension characterization

Cr<sub>2</sub>O<sub>3</sub> NPs were purchased from Jianglai Biology Ltd., Shanghai, China. The morphology of the Cr<sub>2</sub>O<sub>3</sub> NPs was examined by transmission electron microscopy, operated at 200 kV, and the characteristics of Cr<sub>2</sub>O<sub>3</sub> NPs (0.05 μm) are shown in Fig. S1. Cr<sub>2</sub>O<sub>3</sub> NPs of different concentrations were added to nutrient solution and agitated by ultrasonic vibration (100 W, 40 kHz) for 30 min to increase dispersion. The stability of NPs in the nutrient solution dispersion system was determined by Zeta potential.

### Germination experiment

Soybean seeds were sterilized by 0.7% NaClO solution for 10 min, and then rinsed with deionized water for three times to ensure that the surface was clean. Then the seeds were immersed in Cr<sub>2</sub>O<sub>3</sub> NP-water with different concentrations

of suspension (CK, 0.01, 0.05, 0.1, and 0.5 g L<sup>-1</sup>), and subsequently placed in the dark at 25 °C, making sure that the seeds maintained humidity. After germination (3d), the germination rate was calculated.

### Plant culture

Soybean seeds were rinsed with deionized water for three times after sterilizing by 0.7% NaClO solution for 10 min. Then the seeds were immersed in deionized water for germination, and subsequently placed in the dark at 25 °C, making sure the seeds maintained humidity. After 3 days, buds whose lengths surpassed half of the seed length were chosen and then placed to the nutrient solution with the addition of Cr<sub>2</sub>O<sub>3</sub> NPs and cultured under natural conditions.

Uniform seedlings were selected and moved to plastic containers amended with strength of the following nutrient solution (mmol L<sup>-1</sup>): Ca(NO<sub>3</sub>)<sub>2</sub>, 2.0; KH<sub>2</sub>PO<sub>4</sub>, 0.1; MgSO<sub>4</sub>, 0.5; KCl, 0.1; K<sub>2</sub>SO<sub>4</sub>, 0.7; H<sub>3</sub>BO<sub>3</sub>, 10 × 10<sup>-3</sup>; MnSO<sub>4</sub>, 5 × 10<sup>-4</sup>; ZnSO<sub>4</sub>, 5 × 10<sup>-4</sup>; CuSO<sub>4</sub>, 2 × 10<sup>-4</sup>; (NH<sub>4</sub>)<sub>6</sub>MoO<sub>24</sub>, 1 × 10<sup>-4</sup>; and Fe-EDTA, 20 × 10<sup>-3</sup>. Cr<sub>2</sub>O<sub>3</sub> NPs were added to the nutrient solution, and five experimental treatment groups were initiated (g L<sup>-1</sup>): 0.01, 0.05, 0.1, 0.5, and control (CK). The pH of the nutrient solution was adjusted to 6.0. Each experiment had four replicates. The seedlings grew for 14 days under natural conditions: at 25–30/20–25 °C (day/night) with relative humidity at 60–70% and a light intensity at 15,000 lx. The suspensions with NPs were renewed every 3 days. The exposure time was 14 days; shoot and root tissue were washed by ultrasonic vibration (output frequency 53 kHz, power 500 W, SK20GT, Ishine, China) to remove the NPs on the surface, subsequently separated and dried by Bal-Tec CPD 030 a critical point dryer (Leica, Wetzlar, Germany) at 65 °C for 72 h. Fresh biomass of shoots and roots of tissues from all treatments were measured, and Cr content in plant tissues were analyzed by ICP-MS (Agilent 7500a, USA) after digestion with HNO<sub>3</sub>-HClO<sub>4</sub>.

### SEM-EDS and TEM observation

SEM-EDS was performed to observe the transport of nanoparticles in plants and their effects on plant morphology. TEM was used to analyze the structure change of chloroplast, thus revealing the reasons for inhibition of photosynthetic system.

Fresh soybean root and shoot tissues were separated, and the shoots were placed in 4 °C refrigerator to avoid light overnight for dark recovery. The samples were first fixed with 2.5% glutaraldehyde in phosphate buffer (0.1 M, pH 7.0) for more than 4 h, washed three times in the phosphate buffer (0.1 M, pH 7.0) for 15 min at each step, then post fixed with 1% OsO<sub>4</sub> in phosphate buffer for 1–2 h and washed three times in the phosphate buffer (0.1 M, pH 7.0) for 15 min at each step. The samples were prepared for dehydration: the

samples were first dehydrated by graded series of ethanol (30, 50, 70, 80, 90, 95, and 100%) for about 15 to 20 min at each step.

For SEM scanning, the samples were transferred to the mixture of alcohol and iso-amyl acetate (v:v = 1:1) for about 30 min, and then transferred to pure iso-amyl acetate for about 1 h. In the end, the samples were dehydrated in Hitachi Model HCP-2 critical point dryer with liquid CO<sub>2</sub>. The dehydrated samples were coated with gold-palladium in Hitachi Model E-1010 ion sputter for 4–5 min and observed in Hitachi Model TEM-1000 SEM and INCA100 EDS (Oxfordshire, UK).

For TEM scanning, the specimen was placed in 1:1 mixture of absolute acetone and the final Spurr resin mixture for 1 h at room temperature, then transferred to 1:3 mixture of absolute acetone and the final resin mixture for 3 h and lastly to the final Spurr resin mixture for overnight. The specimen was placed in Eppendorf contained Spurr resin and heated at 70 °C for more than 9 h. The specimen was sectioned in LEICA EM UC7 ultratome and sections were stained by uranyl acetate and alkaline lead citrate for 5 to 10 min, respectively, and observed in Hitachi Model H-7650 TEM.

### Chlorophyll fluorescence measurement

After being cultured in complete nutrient solution with Cr<sub>2</sub>O<sub>3</sub> NPs, the samples were picked and ready to be used to evaluate the effect of Cr<sub>2</sub>O<sub>3</sub> NPs on PSII electron transport. Soybean leaves were placed in the dark for 30 min for dark adaptation, CF Imager (CF0056, TNC, America) was used to evaluate the dark reaction efficiency. Readings of dark-adapted minimum fluorescence (Fo), dark-adapted maximum fluorescence (Fm), variable fluorescence Fv (Fv = Fm - Fo) were recorded. Fo' and Fm' were measured by CF Imager after 30 min of light intensity of 1000 μmol (m<sup>2</sup> s)<sup>-1</sup>. Data of potential capture efficiencies Fv/Fm (XE), non-photochemical quenching Fm/Fm'-1 (NPQ) and the capture rate of excitation energy of PSII reaction center Fv'/Fm (XE'), photochemical quenching coefficients Fq'/Fv (qP) and Fq'/Fm' (φPSII) were recorded. State was ready for monitoring in leaves *in vivo* with CF Imager. All the leaves were measured under the same condition.

Photosynthesis rate, intercellular CO<sub>2</sub> concentration, and stomatal conductance were measured by using the LI-6400/LI-6400XT Portable Photosynthesis System (LI-6400XT; Li-Cor Environmental, Lincoln, NE, USA).

### Activity of the photosynthetic enzyme (MDH, Rubisco) and determination of chlorophyll content

This experiment adopted the tissue kit (Suzhou Comin Biotechnology Co. Ltd) and followed the protocol provided to measure the activity of Rubisco (Rubisco, EC 4.1.1.39) in soybean leaves.

Malate dehydrogenase (MDH) tissue kit was from Nanjing Jiancheng Bioengineering Institute, and the activity of MDH was examined according to the protocol provided (Lv et al. 2013).

Fresh soybean leaves were collected and washed for sampling. A mass of 0.1 g crushed leaves were put into 25 mL colorimetric tube and 15 mL of extract (acetone:ethanol = 1:1) were added. After 24-h of dark soaking, the leaves turned to be transparent. The extract was used as blank control. Chlorophyll was examined by spectrophotometer (721–100) at the wavelength of 649 and 665 nm.

### Statistical analysis

Data were analyzed statistically using the SPSS package (version 11.0; SPSS Inc., Chicago, IL, USA). Analysis of variance (ANOVA) was performed on the datasets. Means of significant difference were separated by *t* test or Duncan’s multiple range test at the  $p < 0.05$  level.

## Results

### NP characterization

The characterization of Cr<sub>2</sub>O<sub>3</sub> NPs was determined by Zeta potential and TEM. The stability of NP suspensions was

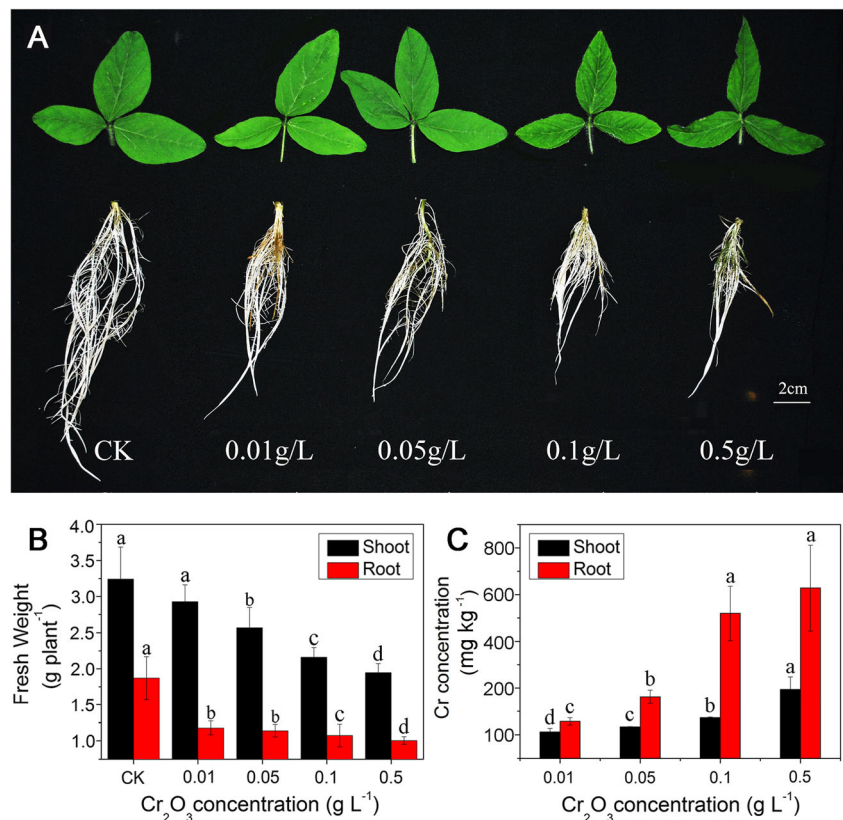
increasing with the growing concentrations as shown in Table S1. Ion release of the Cr<sub>2</sub>O<sub>3</sub> NP-nutrient solution was under 0.02 mg kg<sup>-1</sup> before plant culture, and it was stable around 0.033 mg kg<sup>-1</sup> at harvest. The NP aggregate morphology is shown in Fig. S1a, the size of which was around 500 nm, while the original size of Cr<sub>2</sub>O<sub>3</sub> NPs was around 30–50 nm (Fig. S1b), and the original size of which meets the experimental requirements.

### Seed germination, growth inhibition and metal accumulation

Seed germination and plant growth experiment were conducted. Cr<sub>2</sub>O<sub>3</sub> NPs were not influential to soybean seed germination ( $p < 0.05$ ) (Fig. S2).

Plant growth was inhibited significantly when exposed to Cr<sub>2</sub>O<sub>3</sub> NPs, and leaf malformation was observed when Cr<sub>2</sub>O<sub>3</sub> NP level  $\geq 0.1$  g L<sup>-1</sup> (Fig. 1a). Comparing with control treatment, shoot fresh weights at Cr<sub>2</sub>O<sub>3</sub> NP treatments (0.01, 0.05, 0.1, and 0.5 g L<sup>-1</sup>) were decreased by 9.6, 20.9, 33, and 40.1%, respectively, and the corresponding values for root fresh weight were 39.1, 37.1, 42.6, and 46.4%, respectively. Plant morphology changes were visible. At high concentrations (0.1 and 0.5 g L<sup>-1</sup>), the soybean foliage became slender and more wrinkles appeared. Root growth was inhibited as well. Under the high concentration of nanoparticle solution,

**Fig. 1** Effect of Cr<sub>2</sub>O<sub>3</sub> NPs on plant growth (a), biomass (b), and Cr contents in shoot and root (c). Soybean plants were treated with different Cr<sub>2</sub>O<sub>3</sub> NP levels. The image was taken on the 14th day of treatment, and biomass and Cr concentration were analyzed. Data are means  $\pm$  SD ( $n = 4$ ). Bars with different letters are significantly different at  $p < 0.05$



the roots were swollen with root elongation inhibited, and the number of lateral roots was less than that of the control group.

The Cr content in shoots and roots of soybean increased along with the  $\text{Cr}_2\text{O}_3$  NPs level (Fig. 1c). Cr content of the roots was significantly higher than that of the shoots. In the low concentration fraction, there was little difference in the uptake of metals in the shoots, but when the concentration reached  $0.1 \text{ g L}^{-1}$ , the metal content of the shoots was quite different. At  $0.5 \text{ g L}^{-1}$ , the Cr content was much higher than the content of  $0.01 \text{ g L}^{-1}$ . And the root Cr concentration also increased with the increase of the concentration of the nanoparticle dispersion.

### Xylem transport of $\text{Cr}_2\text{O}_3$ NPs and root morphology changes

Scanning electron microscopy along with EDS was conducted to determine the root and stem growth of the group exposed to  $0.5 \text{ g L}^{-1}$   $\text{Cr}_2\text{O}_3$  NPs. The root surface of the control group was texture clear, and the lateral roots and root hairs could be seen under the SEM view. The cortical, endocortical, and

xylem ducts were found from the section view of the stem of the soybean (Fig. 2a), and the root size was normal. As for the high  $\text{Cr}_2\text{O}_3$  NPs exposure group, a large number of NPs can be seen under high power lens (Fig. 3d). These nanoparticles were gathered and remained on the surface, the size of which were hundred and thousand times of their original size. The roots and lateral roots of the experimental group were swollen (Fig. 3), the surface of which were covered by  $\text{Cr}_2\text{O}_3$  NPs, and the root hair can hardly be seen at high magnification. The stem section diagram of the high exposure group is shown in Fig. 2b, in which the xylem catheters were attached by a large number of particles (Fig. 2c, d); the massive particles adhered to the xylem catheter and the phloem catheter were proved to be  $\text{Cr}_2\text{O}_3$  NPs by EDS.

### Chlorophyll fluorescence

After 14 days of growth in the nutrient solutions containing five different  $\text{Cr}_2\text{O}_3$  NPs concentrations, the chlorophyll fluorescence parameters of soybean leaves were measured (Fig. 4). When the leaf was illuminated, the darker part of

**Fig. 2** SEM observation of stem cross-section. **a** Control group; **b** after treated with  $0.5 \text{ g L}^{-1}$   $\text{Cr}_2\text{O}_3$  NPs for 14 days; **c, d** enlarged view of **(b)**; **e** particle analysis of EDS

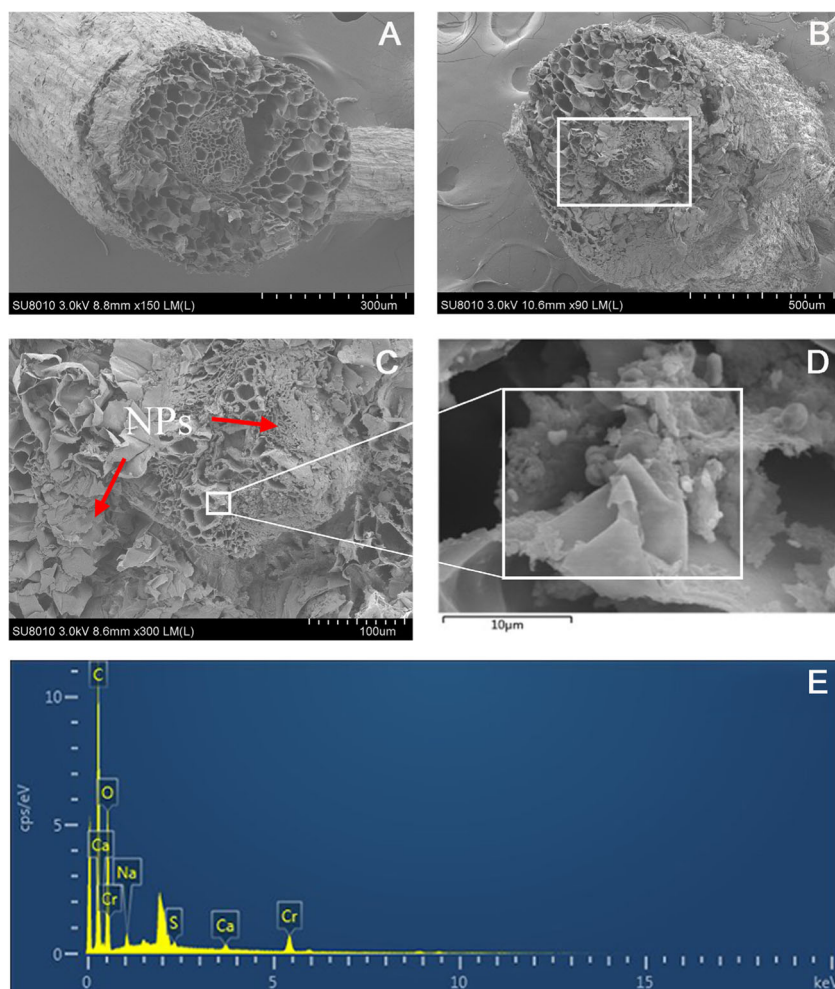
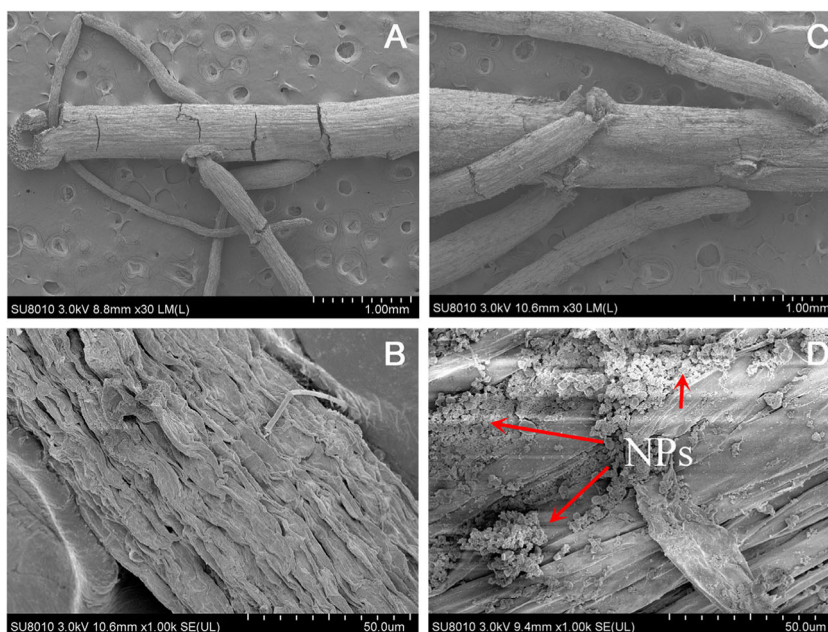


**Fig. 3** SEM observation of root surface. **a** Control group; **b** enlarged view of control group; **c** after treated with Cr<sub>2</sub>O<sub>3</sub> NPs for 14 days; **d** enlarged view of exposure group



the image provided evidence for leaf damage in the Fq/Fm', reflecting an inhibition of both photochemical and non-photochemical PSII processes (Fig. 4b); the data reflected a downward trend except for the 0.1-g L<sup>-1</sup> group. After 30 min dark recovery (Fig. 4a), the maximum quantum yield of the controlled group of PSII (Fv/Fm) was 0.854, while the test group results were all lower than it (*p* value < 0.05.), which indicated that non-photochemical quenching has reversed and decreased during the dark period with the growing concentration of NPs. As compared with CK, the qP decreased by 30, 30, 32, and 37%, respectively. The NPQ were increased gradually, which indicated the heat dissipation of leaves increased with the rise of the NP concentrations.

**Photosynthetic parameters and activity photosynthetic enzymes (MDH and Rubisco)**

Intercellular CO<sub>2</sub> concentration (Fig. 5) decreased gradually from 335 to 268 μmol CO<sub>2</sub> mol<sup>-1</sup>, and the reduction rate was 6.9, 9.4, 15.8, and 19.7%, respectively, indicating the available CO<sub>2</sub> was lowered due to the stronger respiration (NPQ, Fig. 4). As shown in Fig. 5, leaf conductance to H<sub>2</sub>O decreased (except the stomatal conductance of group 0.01 g L<sup>-1</sup>), and this result was closely related to photosynthetic rate, which showed a downslope similarly (Fig. S2), ranging from the control group 11.46 μmol CO<sub>2</sub> m<sup>-2</sup> s<sup>-1</sup> to the experimental group 9.59, 9.41, 8.73, and 7.68 μmol CO<sub>2</sub> m<sup>-2</sup> s<sup>-1</sup>, respectively. Strong reduced activity of both MDH and Rubisco were observed in soybean groups grown in the presence of NPs compared with the control treatment. As shown in Fig. 5b, MDH activity decrease began from 4.62 to 3.39 U mg<sup>-1</sup> prot<sup>-1</sup>, then reduced by 77.4, 90.8, and 96.5%

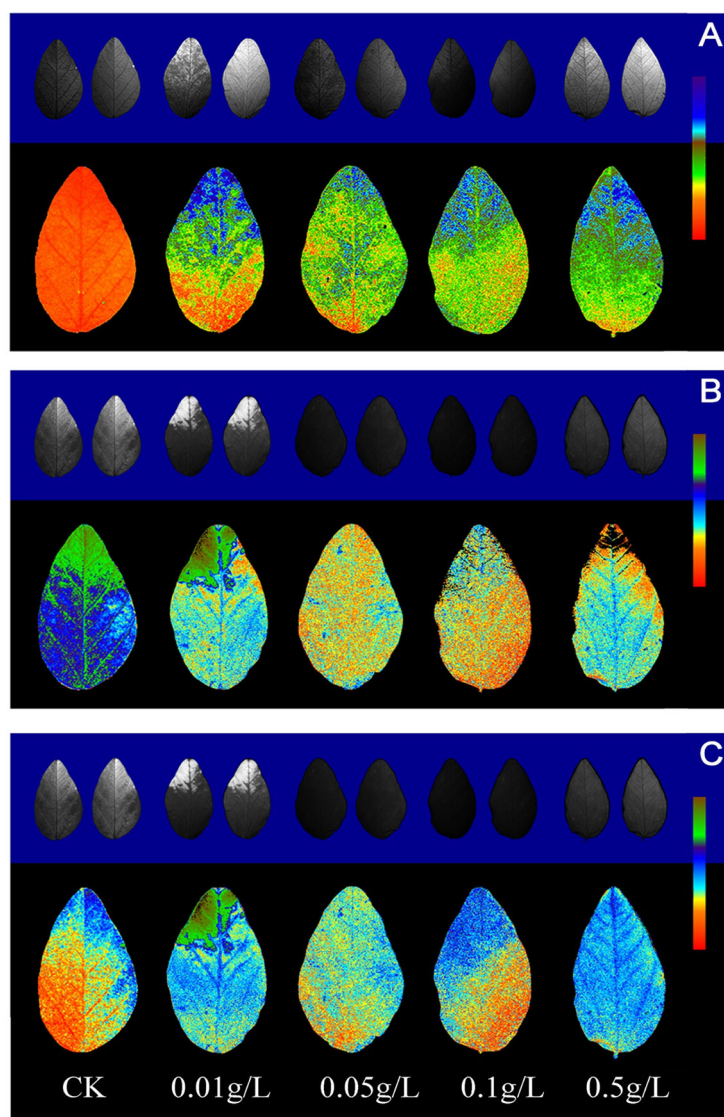
(1.04, 0.42, and 0.16 U mg<sup>-1</sup> prot<sup>-1</sup>, respectively). This downward trend became slow when the NP concentration reached 0.05 g L<sup>-1</sup>, meanwhile Rubisco activity (Fig. 5a) similarly showed a rapid decline with the addition of NPs (CK, 95.3 nmol min<sup>-1</sup> g<sup>-1</sup>; reduction rate, 54.5, 72.7, 81.8, and 86.4%, respectively) and then kept closely to 10 nmol min<sup>-1</sup> g<sup>-1</sup>. The effect that NPs posed to photosynthetic enzymes was debased after the NP concentration rose to a certain degree.

**Photosynthetic pigments and TEM observation**

Soybean grown in Cr<sub>2</sub>O<sub>3</sub> NPs had a significant reduction in chlorophylls *a* and *b* compared with those grown in the nutrient solution (Table 1). With the increase of the concentration, the chlorophyll content of plants decreased and the growth of plants became weaker, with shorter root elongation and relatively smaller and narrower leaves (Fig. 1c), providing evidence that Cr<sub>2</sub>O<sub>3</sub> NPs had negative effect on the photosynthesis of soybean leaves.

Transmission electron microscopy was used to analyze the ultrastructure structures of the high-concentration group (Cr<sub>2</sub>O<sub>3</sub> NPs, 0.5 g L<sup>-1</sup>). As for the control group (Fig. 6a), the cells observed under transmission electron microscope were complete, the grana stacking in the chloroplasts were clear as well, and starch granules were evenly distributed between the grana. As for the high Cr<sub>2</sub>O<sub>3</sub> NP concentration exposure group (Fig. 6b), the vacuole in the cell was relatively larger than the control group. The grana stacking was broken and relatively more starch granules can be observed. Under the TEM, one special cell was found in which the chloroplast

**Fig. 4** Effect of different  $\text{Cr}_2\text{O}_3$  NP-level treatment on the maximum quantum yield of PSII ( $F_v/F_m$ ), photochemical quenching ( $qP$ ), and non-photochemical quenching (NPQ) of intact leaves. The images were taken by CF Imager on the 14th day of treatment. **a** Leaf damage evaluation mapping based on potential energy capture efficiency of the reaction center after dark recovery for 30 min. The specific color band from red to dark blue stated the leaf damage from slight to severe. **b** Leaf damage evaluation mapping based on non-photochemical quenching NPQ under illumination. The specific color band from light green to red stated the leaf damage from slight to severe. **c** Leaf damage evaluation mapping based on photosynthesis quenching coefficient  $qP$ . The specific color band from red to light green stated the efficiency from high to low. Data are means  $\pm$  SD ( $n = 3$ ). Data with different letters are significantly different at  $p < 0.05$



Treatment	$F_v/F_m$	$F_q'/F_v'$	$F_q'/F_m'$	NPQ	$qP$
$\text{Cr}_2\text{O}_3$ g L <sup>-1</sup>					
CK	0.854 $\pm$ 0.011a	0.656 $\pm$ 0.0041a	0.778 $\pm$ 0.008a	1.496 $\pm$ 0.012a	0.66 $\pm$ 0.01a
0.01	0.786 $\pm$ 0.009b	0.455 $\pm$ 0.015b	0.652 $\pm$ 0.012b	2.123 $\pm$ 0.004b	0.46 $\pm$ 0.01b
0.05	0.759 $\pm$ 0.013c	0.469 $\pm$ 0.008c	0.627 $\pm$ 0.003c	2.374 $\pm$ 0.006c	0.46 $\pm$ 0.02c
0.1	0.697 $\pm$ 0.009d	0.445 $\pm$ 0.007d	0.554 $\pm$ 0.006d	2.487 $\pm$ 0.011d	0.45 $\pm$ 0.02d
0.5	0.667 $\pm$ 0.006d	0.409 $\pm$ 0.005d	0.603 $\pm$ 0.009cd	2.473 $\pm$ 0.004d	0.41 $\pm$ 0.01d

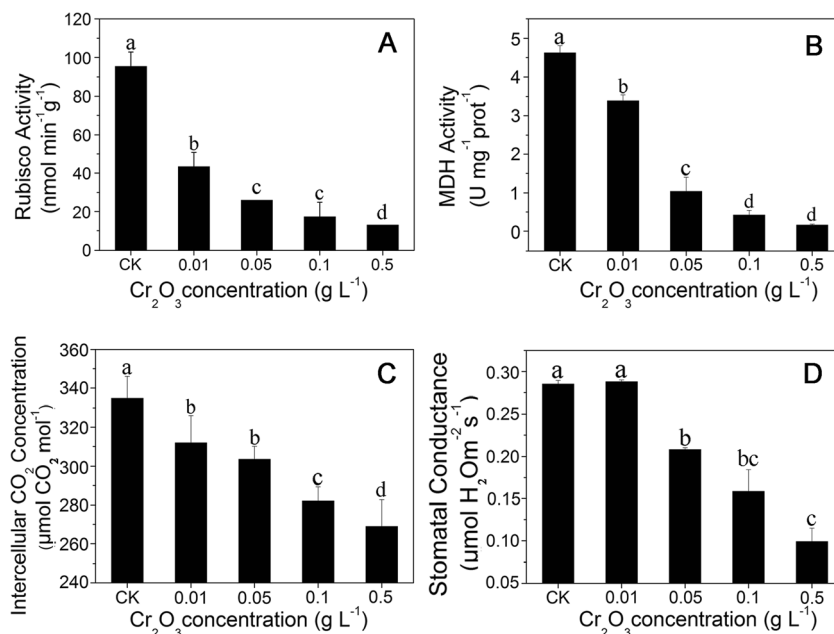
particles were completely broken and the chloroplasts were completely encapsulated by the starch granules (Fig. 6e).

## Discussion

In recent years, several investigators have shown impact of nanoparticles on plant growth and their accumulation in food

source (Anshu et al. 2017), but few studies addressing the toxic potential of these NPs have been reported in the literature (Puerari et al. 2016). The problems caused by industrial wastewater discharge have been constant issues under the present circumstances. Once the crops were contaminated by industrial wastewater with large quantity of high NPs (such as  $\text{Cr}_2\text{O}_3$ ) in a short term, our research will provide insights for the research on the hazards of  $\text{Cr}_2\text{O}_3$  NP pollution.

**Fig. 5** Effect of Cr<sub>2</sub>O<sub>3</sub> NPs on rubisco activity (a), MDH activity (b), intercellular CO<sub>2</sub> concentration (c), and stomatal conductance(d) of soybean leaves. Soybean plants were treated with different Cr<sub>2</sub>O<sub>3</sub> NP levels. Data are means ± SD (n = 4). Bars with different letters are significantly different at p < 0.05



Cr<sub>2</sub>O<sub>3</sub> NPs were found to adhere and aggregate in soybean plants (Figs. 2 and 3), and this is a direct evidence that Cr<sub>2</sub>O<sub>3</sub> NPs can be absorbed and transported by soybean plants, which also indicated the potential problems caused by NPs. Also, soybean phloem catheter a small amount of nanoparticles, indicating that nanoparticles can be transferred down through the phloem (Fig. 2c), which is consistent with the previous report (Ma et al. 2015). The cross-section showed that NPs are gathered in the xylem and phloem in the stem, indicating an up-and-down transfer inside the plants. This mechanism may contribute to protection of plants from heavy metal toxicity. To determine the uptake and accumulation of NPs by plants that show consistency with previous studies (Ma et al. 2015), we examined photosynthetic and morphology changes that NPs posed to plants as well.

**Soybean plant growth were inhibited under the exposure of Cr<sub>2</sub>O<sub>3</sub> NPs**

Consistently with previous research (Ma et al. 2015), seed germination was not sensitive to Cr<sub>2</sub>O<sub>3</sub> NPs under all levels

in this study. This may have related to the seed coat, which has selective permeability and can protect the embryo from external toxicity (Dimkpa et al. 2012). However, the influence on mature plants is different after being exposed to Cr<sub>2</sub>O<sub>3</sub> NPs for 14 days of treatment. According to ICP-MS data, the uptake of Cr<sub>2</sub>O<sub>3</sub> NPs in roots showed a positive correlation with the concentration, which indicate that the root elongation of soybean is affected by the content of Cr<sub>2</sub>O<sub>3</sub> NPs absorbed by plants. Besides, roots growth showed an inhibition in early growth stage at a low level of NPs, and tissue morphology changes were visible. As for the roots, our study found that the roots were shorter and swelled with less lateral roots. Liu et al. (2010) found that NPs can induce swollen roots by affecting isotropic growth of epidermal cells, auxin disruption, and aberrant microtubule arrangement as well as cell division, causing root morphology changes. On the other hand, the uptake of Cr<sub>2</sub>O<sub>3</sub> NPs in shoots was only significant at high concentrations. In agreement with root morphology changes, leaf areas were shrunk with the growing concentration of Cr<sub>2</sub>O<sub>3</sub> NPs. The estimation of total leaf areas indicated that the plant health was affected by the water

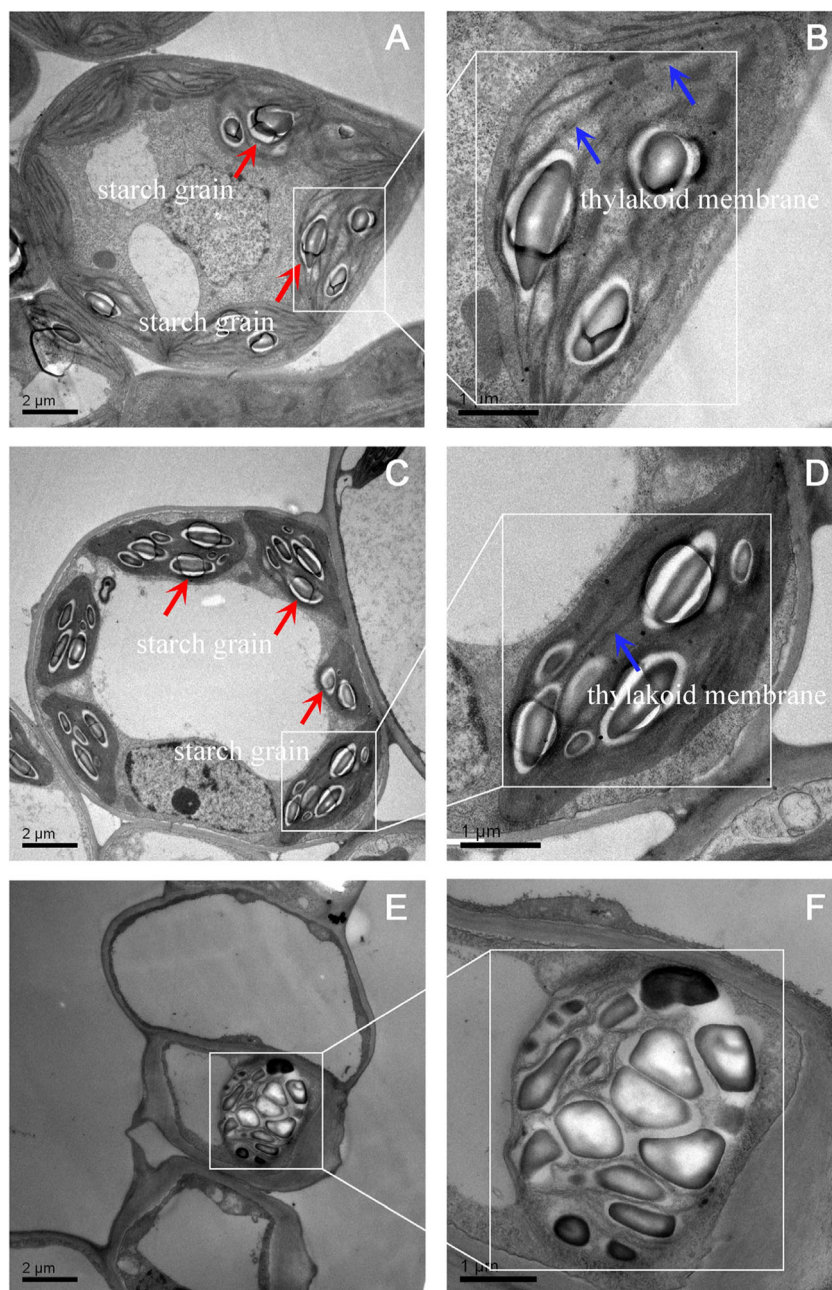
**Table 1** Effect of Cr<sub>2</sub>O<sub>3</sub> NPs on the concentrations of chlorophylls a and b in fresh leaves

Treatment Cr <sub>2</sub> O <sub>3</sub> (g L <sup>-1</sup> )	Chlorophyll a (mg g <sup>-1</sup> )	Chlorophyll b (mg g <sup>-1</sup> )	a/b ratio
Control	0.925 ± 0.38 a	0.587 ± 0.21 a	1.57 ± 0.08 a
0.01	0.836 ± 0.04 b	0.524 ± 0.14 b	1.59 ± 0.04 a
0.05	0.819 ± 0.035 b	0.489 ± 0.11 b	1.67 ± 0.03 ab
0.1	0.784 ± 0.19 b	0.447 ± 0.25 c	1.75 ± 0.06 b
0.5	0.608 ± 0.17 c	0.346 ± 0.29 d	1.76 ± 0.11 b

Soybean plants were treated with different Cr<sub>2</sub>O<sub>3</sub> NP levels. On the 14th day of treatment, chlorophyll concentrations were analyzed. Data are means ± SD (n = 4). Bars with different letters are significantly different at p < 0.05



**Fig. 6** Effect of  $\text{Cr}_2\text{O}_3$  NPs on chloroplast ultrastructure of leaf cells of soybean treated with or without  $\text{Cr}_2\text{O}_3$  NPs. The TEM images were taken on the 14th day of treatment. **a, b** Control; **c, d** treated by  $500 \text{ mg L}^{-1}$   $\text{Cr}_2\text{O}_3$  NPs. **e, f** chloroplast of treated group full of starch grains and destroyed grana. Red narrow-pointed starch grains. Blue narrow-pointed thylakoid membrane



stress (Gutiérrez-Boem and Thomas 2001) and the metal exposure (Weryszko-Chmielewska and Chwil 2005). Previous research supported our findings that nanoparticles can be gathered into a group in the surface of plant, clogging root transport channels of water and ion, inhibiting root hydraulic conductivity and nutrient absorption (Adani et al. 2010). These findings are consistent with our observations that NPs can directly lead to the shorter root elongation and the shrunken leaf area of the plant.

However, the reason for the decrease of plant biomass and the narrower shape of leaves with increasing concentration has not been fully understood yet and needs further study.

### Photosynthetic damage of soybean plants exposed to $\text{Cr}_2\text{O}_3$ NPs based on chlorophyll fluorescence

Chlorophyll fluorescence analysis has become one of the most powerful technique to estimate the photochemical activities of PSII in leaves and the operating quantum efficiency of electron transport through PSII (Baker and Rosenqvist 2004), which can provide insight into intra-cellular photosynthetic responses to abiotic stress (Seaton and Walker 1990).

Consistently with Perreault et al. (2010), NPs induced photosynthetic decrease was remarkable according to the photosynthetic parameters taken by a CF imager. The maximum

quantum yield of PSII (Fv/Fm) can reflect a dissociation of light harvesting pigment systems of PSII from PSII core (Murchie and Lawson 2013). According to Fig. 4a, b, the dark response of the plant was inhibited and the light system was also reduced with the addition of Cr<sub>2</sub>O<sub>3</sub> NPs and showed a reduction along with the concentration, which was similar to CuO NPs induced by photosynthetic inhibition (Perreault et al. 2010). The process of NPQ is regulated by the acidification of the thylakoid lumen due to the accumulation of protons in the thylakoid lumen (during linear and cyclic electron flow) that forms a  $\Delta$ pH (Ruban et al. 2012). The outcome of both qP and NPQ suggested that the respiration intensity was promoted while the access to the photochemical center was suppressed (Oxborough and Baker 1997). Stomatal conductance and intercellular CO<sub>2</sub> were measured to confirm the hypothesis. In conclusion, plant respiration increased along with the concentration of Cr<sub>2</sub>O<sub>3</sub> NPs, which indicated a consumption of plant energy and a reduction of CO<sub>2</sub> content, thereby affecting the photosynthesis.

Results showed that Cr<sub>2</sub>O<sub>3</sub> NPs can inhibit the ability of plant to produce chlorophylls *a* and *b*, thus the photosynthetic procedure could be reduced by the lack of raw materials (Anderson and Boardman 1966). Aside from the chlorophyll content, plant respiration, and the capacity for photochemistry, electron transportation, on the other hand, also plays an essential role in the photosynthetic system. PSII quantum efficiency (Fq'/Fm') theoretically measured the proportion of the light absorbed by photosystem II that is used in photochemistry, and it could indicate the mass level of electron acceptors (NADP<sup>+</sup>) at the acceptor side of PSI (Murchie and Lawson 2013). According to chlorophyll fluorescence mapping, we can infer that electron transportation was inhibited in photosynthesis, which was connected with the existence of Cr<sub>2</sub>O<sub>3</sub> NPs, but no concentration-dependent relation was being showed. The interruption of energy transfer can be determined by the activity of the enzyme. Rubisco and Malate dehydrogenase are related to the abundance of photosynthesis-related proteins (Murchie and Lawson 2013). Ribulose-1,5-bisphosphate carboxylase/oxygenase is a key enzyme in the plant photosynthetic procedure (Lin et al. 2014), controlling the fixing ability of CO<sub>2</sub> fixation, meanwhile, restricting and splitting carbon to the Calvin cycle and photorespiration cycle (Buchanan and Balmer 2005), the activity of which directly influences the rate of photosynthesis. In photorespiration, MDH provides NAD<sup>+</sup> for oxidation of Gly (glycine) (Hatch et al. 1982; Moreadith and Lehninger 1984; Gietl 1992). According to Fig. 5a, b, the activity of the enzymes confirmed that Cr<sub>2</sub>O<sub>3</sub> NPs could inhibit the electron transportation during the optoelectronic circulation of PSI, causing damage to the photosynthetic system, thus reducing the photosynthesis rate of soybean

plants. Since the enzyme activity of photosynthetic system is affected, chloroplasts of soybean plants may also be affected or even destroyed (Redondo-Gómez et al. 2010), thus we took chloroplasts into further consideration.

Chloroplasts were observed under TEM. Starch grains are produced during the photoreaction stage to store the energy, and they will be delivered to dark reaction for the Calvin cycle (Slack et al. 1969). Thus, the amount of starch granules can be used to assess the circulation of the cycle system. From Fig. 6, the exposure group showed more starch grains and less grana, and a deformed chloroplast was observed under TEM, whose structure was totally destroyed, suggesting the damage of the structure of chloroplast was induced by Cr<sub>2</sub>O<sub>3</sub> NPs. Based on the previous data of Rubisco and MDH activity and TEM observation, the conversion process from C5 to C3 of Calvin cycle was influenced with the inhibition electron transportation.

It can be said that once Cr<sub>2</sub>O<sub>3</sub> NP-contaminated water are absorbed by plants, the plants will show different degrees of inhibition on growth and photosynthesis at different concentrations. The growth and morphology changes happened mainly through the blockage of plant nutrient absorption channel as well as by reducing the enzyme activity which to the reduce and even suspend the energy conversion during Calvin cycle, so that the starch granules cannot be decomposed in the chloroplast thus destroying the chloroplast ultrastructure, resulting in reduced photosynthetic efficiency.

## Conclusion

The findings of this research revealed that Cr<sub>2</sub>O<sub>3</sub> NPs can be absorbed by soybean plants through xylem, causing root swelling and affecting the growth of plants by (1) inhibiting the activity of photosynthetic enzymes and causing a low conversion efficiency of C5 to C3 in Calvin cycle; (2) increasing the starch grains and breaking the thylakoid membrane, consequently destructing the substructure of chloroplasts of soybean plants; (3) blocking the level of electron acceptors (NADP<sup>+</sup>) at the acceptor side of PSI transport during photosynthetic process, reducing the formation and activity of chlorophyll, and posing irreversible damage to plants. However, a further study of Cr<sub>2</sub>O<sub>3</sub> NPs and its fate in soil is needed to understand the behavioral differences between the changes in the external environment. The information obtained from this continuation will help to understand the fate and transport of Cr<sub>2</sub>O<sub>3</sub> NPs and assess the potential food safety risks associated with the consumption of soybean or other edible plants grown in the presence of Cr<sub>2</sub>O<sub>3</sub> nanoparticle-contaminated industrial wastewater.

**Acknowledgements** The authors are grateful to Ms. Si Li of the technician of 985-Institute of Agrobiological and Environmental Sciences of Zhejiang University for her contribution in carrying through the in situ hybridization.

**Funding information** This study was financially supported by the National Natural Science Foundation of China (No. 41271333, No. 21477104, No. 41671315) and National Key Research and Development Projects of China (No. 2016YFD0800802).

## References

- Adani F, Papa G, Schievano A, Cardinale G, D'Imporzano G, Tambone F (2010) Nanoscale structure of the cell wall protecting cellulose from enzyme attack. *Environ Sci Technol* 45(3):1107–1113
- Anderson JM, Boardman N (1966) Fractionation of the photochemical systems of photosynthesis I. Chlorophyll contents and photochemical activities of particles isolated from spinach chloroplasts. *Biochim Biophys Acta* 112(3):403–421
- Anshu R, Marek Z, Oksana S, Kalaji HM, He X, Sonia M et al (2017) Impact of metal and metal oxide nanoparticles on plant: a critical review. *Front Chem* 5:78
- Baker NR, Rosenqvist E (2004) Applications of chlorophyll fluorescence can improve crop production strategies: an examination of future possibilities. *J Exp Bot* 55(403):1607–1621
- Birbaum K, Brogioli R, Schellenberg M, Martinoia E, Stark WJ, Günther D, Limbach LK (2010) No evidence for cerium dioxide nanoparticle translocation in maize plants. *Environ Sci Technol* 44(22):8718–8723
- Buchanan BB, Balmer Y (2005) Redox regulation: a broadening horizon. *Annu Rev Plant Biol* 56:187–220
- Cui D, Zhang P, Ma Y, He X, Li Y, Zhang J, Zhang Z (2014) Effect of cerium oxide nanoparticles on asparagus lettuce cultured in an agar medium. *Environ Sci Nano* 1(5):459–465
- De La Torre-Roche R, Hawthorne J, Musante C, Xing B, Newman LA, Ma X, White JC (2013) Impact of Ag nanoparticle exposure on *p,p'*-DDE bioaccumulation by *Cucurbita pepo* (zucchini) and *Glycine max* (soybean). *Environ Sci Technol* 47(2):718–725
- Dimkpa CO, McLean JE, Latta DE, Manangón E, Britt DW, Johnson WP, Anderson AJ (2012) CuO and ZnO nanoparticles: phytotoxicity, metal speciation, and induction of oxidative stress in sand-grown wheat. *J Nanopart Res* 14(9):1–15
- Ebbs SD, Bradfield SJ, Kumar P, White JC, Ma X (2016a) Projected dietary intake of zinc, copper, and cerium from consumption of carrot (*Daucus carota*) exposed to metal oxide nanoparticles or metal ions. *Front Plant Sci* 7
- Ebbs SD, Bradfield SJ, Kumar P, White JC, Musante C, Ma X (2016b) Accumulation of zinc, copper, or cerium in carrot (*Daucus carota*) exposed to metal oxide nanoparticles and metal ions. *Environ Sci Nano* 3(1):114–126
- Farinati S, DalCorso G, Panigati M, Furini A (2011) Interaction between selected bacterial strains and *Arabidopsis halleri* modulates shoot proteome and cadmium and zinc accumulation. *J Exp Bot* 62(10):3433–3447
- Gietl C (1992) Malate dehydrogenase isoenzymes: cellular locations and role in the flow of metabolites between the cytoplasm and cell organelles. *BBA-Biomembranes* 1100(3):217–234
- Gutiérrez-Boem FH, Thomas GW (2001) Leaf area development in soybean as affected by phosphorus nutrition and water deficit. *J Plant Nutr* 24(11):1711–1729
- Harris AT, Bali R (2008) On the formation and extent of uptake of silver nanoparticles by live plants. *J Nanopart Res* 10(4):691–695
- Hatch MD, Tsuzuki M, Edwards GE (1982) Determination of NAD malic enzyme in leaves of C4 plants effect of malate dehydrogenase and other factors. *Plant Physiol* 69(2):483–491
- Hawthorne J, De la Torre RR, Xing B, Newman LA, Ma X, Majumdar S, Gardea-Torresdey J, White JC (2014) Particle-size dependent accumulation and trophic transfer of cerium oxide through a terrestrial food chain. *Environ Sci Technol* 48:13102–13109
- Hernandez-Viezas JA, Castillo-Michel H, Andrews JC, Cotte M, Rico C, Peralta-Videa JR, Gardea-Torresdey JL (2013) In situ synchrotron X-ray fluorescence mapping and speciation of CeO<sub>2</sub> and ZnO nanoparticles in soil cultivated soybean (*Glycine max*). *ACS Nano* 7(2):1415–1423
- Kohan-Baghkheirati E, Geisler-Lee J (2015) Gene expression, protein function and pathways of *Arabidopsis thaliana* responding to silver nanoparticles in comparison to silver ions, cold, salt, drought, and heat. *Nano* 5(2):436–467
- Lin MT, Occhialini A, Andralojc PJ, Parry MA, Hanson MR (2014) A faster Rubisco with potential to increase photosynthesis in crops. *Nature* 513(7519):547–550
- Liu Q, Zhao Y, Wan Y, Zheng J, Zhang X, Wang C, Lin J (2010) Study of the inhibitory effect of water-soluble fullerenes on plant growth at the cellular level. *ACS Nano* 4(10):5743–5748
- Lv Y, Liu Z, Tian Y, Chen H (2013) Effect on morphology, oxidative stress and energy metabolism enzymes in the testes of mice after a 13-week oral administration of melamine and cyanuric acid combination. *Regul Toxicol Pharmacol* 65(2):183–188
- Ma X, Geiser-Lee J, Deng Y, Kolmakov A (2010) Interactions between engineered nanoparticles (ENPs) and plants: phytotoxicity, uptake and accumulation. *Sci Total Environ* 408(16):3053–3061
- Ma C, White JC, Dhankher OP, Xing B (2015) Metal-based nanotoxicity and detoxification pathways in higher plants. *Environ Sci Technol* 49(12):7109–7122
- Meshram SP, Adhyapak PV, Mulik UP, Amalnerkar DP (2012) Facile synthesis of CuO nanomorphs and their morphology dependent sunlight driven photocatalytic properties. *Chem Eng J* 204:158–168
- Mirzajani F, Askari H, Hamzelou S, Farzaneh M, Ghassempour A (2013) Effect of silver nanoparticles on *Oryza sativa* L. and its rhizosphere bacteria. *Ecotoxicol Environ Saf* 88:48–54
- Moreadith RA, Lehninger AL (1984) The pathways of glutamate and glutamine oxidation by tumor cell mitochondria. Role of mitochondrial NAD(P)<sup>+</sup>-dependent malic enzyme. *J Biol Chem* 259(10):6215–6221
- Murchie EH, Lawson T (2013) Chlorophyll fluorescence analysis: a guide to good practice and understanding some new applications. *J Exp Bot* 64(13):3983–3998
- Navarro E, Baun A, Behra R, Hartmann NB, Filser J, Miao JA, Sigg L (2008) Environmental behavior and ecotoxicity of engineered nanoparticles to algae, plants, and fungi. *Ecotoxicology* 17(5):372–386
- Ondřej J, Sedmidubský D, Sofer Z, Luxa J, Bartůněk V (2014) Simple synthesis of Cr<sub>2</sub>O<sub>3</sub> nanoparticles with a tunable particle size. *Ceram Int* 41(3):4644–4650
- Oxborough K, Baker NR (1997) Resolving chlorophyll a fluorescence images of photosynthetic efficiency into photochemical and non-photochemical components—calculation of qP and Fv-/Fm-; without measuring Fo. *Photosynth Res* 54(2):135–142
- Park S, Kheel H, Sun GJ, Kim HW, Ko T, Lee C (2016) Room-temperature hydrogen gas sensing properties of the networked Cr<sub>2</sub>. *Met Mater Int* 22(4):730–736
- Parsons JG, Lopez ML, Gonzalez CM, Peralta-Videa JRJL (2010) Toxicity and biotransformation of uncoated and coated nickel hydroxide nanoparticles on mesquite plants. *Environ Toxicol Chem* 29(5):1146–1154
- Perreault F, Oukarroum A, Pirastru L, Sirois L, Gerson Matias W, Popovic R (2010) Evaluation of copper oxide nanoparticles toxicity using chlorophyll fluorescence imaging in *Lemna gibba*. *Aust J Bot*

- Petersen EJ, Henry TB, Zhao J, MacCuspie RI, Kirschling TL, Dobrovolskaia MA, Hackley V XB, White JC (2014) Identification and avoidance of potential artifacts and misinterpretations in nanomaterial ecotoxicity measurements. *Environ Sci Technol* 48:4226–4246
- Priester JH, Ge Y, Mielke RE, Horst AM, Moritz SC, Espinosa K, Schimel JP (2012) Soybean susceptibility to manufactured nanomaterials with evidence for food quality and soil fertility interruption. *PNAS* 109(37):E2451–E2456
- Puerari RC, Costa CHD, Vicentini DS, Fuzinato CF, Melegari SP, Schmidt EC et al (2016) Synthesis, characterization and toxicological evaluation of Cr<sub>2</sub>O<sub>3</sub> nanoparticles using *Daphnia magna*, and *Aliivibrio fischeri*. *Ecotoxicol Environ Saf* 128(June 2016):36–43
- Redondo-Gómez S, Mateos-Naranjo E, Moreno FJ (2010) Physiological characterization of photosynthesis, chloroplast ultrastructure, and nutrient content in bracts and rosette leaves from *glaucium flavum*. *Photosynthetica* 48(4):488–493
- Rickerby DG, Morrison M (2007) Nanotechnology and the environment: a European perspective. *Sci Technol Adv Mater* 8(1):19–24
- Rico CM, Majumdar S, Duarte-Gardea M, Peralta-Videa JR, Gardea-Torresdey JL (2011) Interaction of nanoparticles with edible plants and their possible implications in the food chain. *J Agric Food Chem* 59(8):3485–3498
- Ruban AV, Johnson MP, Duffy CD (2012) The photoprotective molecular switch in the photosystem II antenna. *BBA-Bioenergetics* 1817(1):167–181
- Seaton GGR, Walker DA (1990) Chlorophyll fluorescence as a measure of photosynthetic carbon assimilation. *Proc R Soc B Biol Sci* 242(242):29–35
- Shaw AK, Hossain Z (2013) Impact of nano-CuO stress on rice (*Oryza sativa* L.) seedlings. *Chemosphere* 93(6):906–915
- Slack CR, Hatch MD, Goodchild DJ (1969) Distribution of enzymes in mesophyll and parenchyma-sheath chloroplasts of maize leaves in relation to the C<sub>4</sub>-dicarboxylic acid pathway of photosynthesis. *Biochem J* 114(3):489–498
- Wang Z, Xie X, Zhao J, Liu X, Feng W, White JC, Xing B (2012) Xylem- and phloem-based transport of CuO nanoparticles in maize (*Zea mays* L.). *Environ Sci Technol* 46(8):4434–4441
- Wang P, Menzies NW, Lombi E, McKenna BA, Johannessen B, Glover CJ, Kopittke PM (2013) Fate of ZnO nanoparticles in soils and cowpea (*Vigna unguiculata*). *Environ Sci Technol* 47(23):13822–13830
- Wang Z, Xu L, Zhao J, Wang X, White JC (2016) Xing B (2016) CuO nanoparticle interaction with *Arabidopsis thaliana*: toxicity, parent-progeny transfer, and gene expression. *Environ Sci Technol* 50(11):6008–6016
- Weryszko-Chmielewska E, Chwil M (2005) Lead-induced histological and ultrastructural changes in the leaves of soybean (*Glycine max* (L.)). *Merr Soil Sci Plant Nutr* 51(2):203–212
- Zhai G, Walters KS, Peate DW, Alvarez PJ, Schnoor JL (2014) Transport of gold nanoparticles through plasmodesmata and precipitation of gold ions in woody poplar. *Environ Sci Technol Lett* 1(2):146–151
- Zhang Z, He X, Zhang H, Ma Y, Zhang P, Ding Y, Zhao Y (2011) Uptake and distribution of ceria nanoparticles in cucumber plants. *Metallomics* 3(8):816–822
- Zhao L, Peralta-Videa JR, Ren M, Varela-Ramirez A, Li C, Hernandez-Viezcas JA, Gardea-Torresdey JL (2012) Transport of Zn in a sandy loam soil treated with ZnO NPs and uptake by corn plants: electron microprobe and confocal microscopy studies. *Chem Eng J* 184:1–8
- Zhao L, Sun Y, Hernandez-Viezcas JA, Servin AD, Hong J, Niu G, Gardea-Torresdey JL (2013) Influence of CeO<sub>2</sub> and ZnO nanoparticles on cucumber physiological markers and bioaccumulation of Ce and Zn: a life cycle study. *J Agric Food Chem* 61(49):11945–11951
- Zhu J, Li D, Chen H, Yang X, Lu L, Wang X (2004) Highly dispersed CuO nanoparticles prepared by a novel quick-precipitation method. *Mater Lett* 58(26):3324–3327